A multi-enzyme cascade for efficient production of D-p-hydroxyphenylglycine from L-tyrosine

Xu Tan
School of Pharmaceutical Science, Jiangnan University, Wuxi 214122, China. State Key Laboratory of Food Science and Technology, Jiangnan University, Wuxi 214122, China

Sheng Zhang
Zhejiang Tianrui Chemical Co., Ltd, Quzhou 324400, China

Wei Song
School of Pharmaceutical Science, Jiangnan University, Wuxi 214122, China. State Key Laboratory of Food Science and Technology, Jiangnan University, Wuxi 214122, China

Jia Liu
State Key Laboratory of Food Science and Technology, Jiangnan University, Wuxi 214122, China

Cong Gao
State Key Laboratory of Food Science and Technology, Jiangnan University, Wuxi 214122, China

Xiulai Chen
State Key Laboratory of Food Science and Technology, Jiangnan University, Wuxi 214122, China

Liming Liu
State Key Laboratory of Food Science and Technology, Jiangnan University, Wuxi 214122, China

Jing Wu (wujing@jiangnan.edu.cn)
Jiangnan University

Research

Keywords: D-p-hydroxyphenylglycine, meso-diaminopimelate dehydrogenase, multi-enzyme cascade, hydride transfer distance, L-tyrosine, protein engineering

Posted Date: March 11th, 2021

DOI: https://doi.org/10.21203/rs.3.rs-296444/v1

Abstract

In this study, we designed and *in vivo* reconstructed a novel four-enzyme cascade pathway for the production of D-HPG, a valuable intermediate used to produce β-lactam antibiotics and for fine-chemical synthesis, from L-tyrosine. In this pathway, we identified catalytic conversion of the substrate 4-hydroxyphenylglyoxylic acid by *meso*-diaminopimelate dehydrogenase from *Corynebacterium glutamicum* (*Cg*DAPDH) as the rate-limiting step, followed by application of a mechanism-guided "conformation rotation" strategy to decrease the hydride-transfer distance $d_{(C6HDAP-C4NNADP)}$ and increase *Cg*DAPDH activity. Introduction of the best variant generated by protein engineering (*Cg*DAPDH$^{BC621/D120S/W144S/I169P}$ with 5.32 ± 0.85 U·mg^{-1} specific activity) into the designed pathway resulted in a D-HPG titer of 42.69 g/L from 50 g/L L-tyrosine in 24 h with 92.5% conversion and > 99% *ee* in a 3-L fermenter, representing the highest reported D-HPG titer to date. This four-enzyme cascade provides a novel and effective enzymatic approach to industrial production of D-HPG from cheap amino acids.

Introduction

D-*p*-hydroxyphenylglycine (D-HPG) is an important intermediate widely used in the pharmaceutical and fine-chemical industries for the production of β-lactam antibiotics and aromatic aldehydes (e.g., amoxicillin and 4-hydroxybenzaldehyde, respectively) (Tripathi et al. 2000; Zhang and Cai 2014; Zhang et al. 2010). Currently, D-HPG is in high demand, with a total annual market volume of ~ 5,000 tons (Nandanwar et al. 2013); therefore, development of a practical method for efficient production of D-HPG is required to meet this increasing market demand.

Two main strategies have been developed for D-HPG production: chemical synthesis and enzymatic synthesis. Approaches for chemical synthesis of D-HPG mainly include chiral separation and esterification coupled with hydrolysis (Pollegioni et al. 2020). Using benzenesulfonic acid as a chiral agent, D-HPG can be separated from DL-*p*-hydroxyphenylglycine (DL-HPG) (Zhao and Xu 2015); however, the optical purity of D-HPG obtained by chiral separation is unsatisfactory, with further purification required. Esterification-coupled hydrolysis has emerged to facilitate industrial production of D-HPG. In this process, DL-HPG is first esterified with thionyl chloride to generate DL-HPG methyl ester, followed by hydrolysis to generate D-HPG (Zhang et al. 2011). Alternatively, an enzymatic catalysis strategy involving dual-enzyme synthesis was developed, with this process comprising ring opening of DL-hydroxyphenylhydantoin (DL-HPH) and hydrolysis catalyzed by D-hydantoinase (Hase; EC 3.5.2.2) and N-carbamoyl-D-amino-acid hydrolase (Case; EC 3.5.1.77), respectively (Aranaz et al. 2015; Diez et al. 2015; Liu et al. 2019). A previous study demonstrated this technique in *Escherichia coli* co-expressing Hase and Case, reporting production of 140 mM D-HPG from 140 mM DL-HPH after 32 h with a 100% yield and 0.73 g/L/h productivity (Liu et al. 2019). Unfortunately, the low productivity and high-cost of DL-HPH significantly limit industrial application of this process. Therefore, development of an efficient D-HPG-synthesis method remains challenging.

meso-Diaminopimelate dehydrogenase (DAPDH; EC 1.4.1.16) is an excellent enzyme for use in converting bulky aromatic α-keto acids to corresponding D-amino acids (Ahmed et al. 2015; Gao et al. 2012; Gao et al. 2017). In recent decades, DAPDH catalytic activity toward and substrate affinity for bulky aromatic α-keto acids have improved as a consequence of protein engineering (Akita et al. 2012; Gao et al. 2013; Liu et al. 2014). For example, mutation of *Ureibacillus thermosphaericus* DAPDH (*Ut*DAPDH^{D94A}) resulted in an 8.3-fold increase in enzyme activity toward various bulky α-keto acids, such as phenylpyruvic acid (Hayashi et al. 2017). Similarly, broadening the substrate profile of *Clostridium tetani* E88 DAPDH (*Ct*DAPDH) transformed it from showing no detectable activity toward phenylpyruvic acid to an activity of 0.11 U·mg^{-1} for *Ct*DAPDH$^{Q154L/T173I/R199M/P248S/H249N/N276S}$ (Liu et al. 2015). Therefore, it is possible that DAPDH could be employed to support reductive amination of 4-hydroxyphenylglyoxylic acid (HPGA) to D-HPG.

In this study, we developed a novel cascade pathway allowing transformation of L-tyrosine to D-HPG and reconstructed this pathway *in vivo*. To increase the D-HPG titer, we further developed a mechanism-guided “conformation rotation” strategy to improve the catalytic efficiency of *Cg*DAPDH toward HPGA. The results showed that incorporating the optimal *Cg*DAPDH variant into the cascade pathway enabled synthesis of 42.69 g/L D-HPG from 50 g/L L-tyrosine in 24 h with a 92.5% conversion and > 99% *ee* in a 3-L scale fermenter.

Methods

Reagents and genetic constructions

Commercial reagents, standards, and solvents were purchased from Sigma Aldrich (Shanghai, China), Meryer Chemicals (Shanghai, China), Aladdin Reagents (Shanghai, China), J&K Chemicals (Beijing, China), and TCI Chemicals (Shanghai, China), and used without further purification.

All genetic constructions were carried out by using standard molecular biology techniques with PrimeSTAR and rTaq DNA polymerase, restriction enzymes (SacI, SalI, NdeI, XhoI, HindIII, and EcoRI) and T4 DNA ligase (all from Takara, China). Heterologous genes were amplified from their respective genomic except for *Pv*L-AAD (GenBank: MK258171) and *Pm*L-AAD (GenBank: U35383), which were synthesized by GenScript (Piscataway, NJ). Genes of *Mau*HmaS (GenBank: ADL47009), *Ao*HmaS (GenBank: ANN17105), *Sco*HmaS (GenBank: 1098663), *Sro*HmaS (GenBank: ACZ89671), and *Samb*HmaS (GenBank: AKZ58697) were amplified from the genome of *Micromonospora aurantiaca*, *Amycolatopsis orientalis*, *Streptomyces coelicolor*, *Streptosporangium roseum*, and *Streptomyces ambofaciens*, respectively. Genes of *Hel*MDH (GenBank: CBV41027), *Bgl*MDH (GenBank: AJW98399), *Cs*MDH (GenBank: ABE58432), *Ppu*MDH (GenBank: BAN56662), *Sp*MDH (GenBank: BBD01499), *Cb*MDH (GenBank: CP010537), and *Pa*MDH (GenBank: AGM49308) were amplified from the genome of *Halomonas elongata*, *Burkholderia gladioli*, *Chromohalbacter salexigens*, *Pseudomonas putida*, *Sphingobium* sp., *Cupriavidus basilensis*, and *Pseudomonas aeruginosa*, respectively. Genes of *St*DAPDH (GenBank: BAD40410), *Cg*DAPDH (GenBank: CAF21279), *Bf*DAPDH (GenBank: AKA53147), *Pv*DAPDH (GenBank: ATM98278), and *Pm*DAPDH

(GenBank: CAR40477) were amplified from the genome of *Symbiobacterium thermophilum*, *Corynebacterium glutamicum*, *Bacteroides fragilis*, *Proteus vulgaris*, and *Proteus mirabilis*, respectively.

Strains and plasmids

The host strain *Escherichia coli* BL21 (DE3) was purchased from Invitrogen (Carlsbad, CA, U.S.A.), and was used for all molecular cloning and biotransformation experiments. Gene expression was achieved by cloning the desired gene(s) into a set of plasmids pET28a (+), pETDuet-1, and pACYCDuet-1 (Novagen, Darmstadt, Germany). Main plasmids and strains construction are listed in **Table 1**.

Homology modeling

The 3D homology modeling structures of catalytic domain of *Cg*DAPDH^{BC621} and its variants were constructed using the SWISS-MODEL online server (http://swissmodel.expasy.org/) with DAPDH from *Corynebacterium glutamicum* as template (PDB ID: 5LOA). The obtained structure was verified with SAVES v5.0 (http://servicesn.mbi.ucla.edu/SAVES/). The 3D structure of D-*p*-hydroxyphenylglycine (D-HPG), *p*-hydroxyphenylglyoxylic acid and $NADP^+$ were downloaded from the PubChem Compound (https://www.ncbi.nlm.nih.gov/pccompound/). The analysis of the structures was performed by PyMOL 2.2 (by Schrodinger (SDGR) company). Docking simulations were performed using Autodock Vina and *Cg*DAPDH^{BC621} models.

Molecular dynamics (MD) simulations

The MD simulations were performed using GROMACS (derived from “Not Another Molecular Dynamics program”, by University of Illinois) with the GROMOS96 54a7 force field following the three main steps of energy minimization, system equilibration, and production protocols. After the energy minimization, the systems were gently heated using six 50 ps steps, incrementing the temperature 50 K each step (0-300 K, 30 °C) under constant volume and periodic boundary conditions. Finally, 20 ns MD simulation under NVT ensemble was performed with an integration time step of 2 fs via use of the periodic boundary condition. All simulations were performed individually for both the complexes of *Cg*DAPDH^{BC621} and its mutants. The MD simulations results were analyzed in GROMACS. The difference of root-mean-square deviation (RMSD) between *Cg*DAPDH^{BC621} and *Cg*DAPDH$^{BC621/D120S/W144S/I169P}$ were calculated in the last 15 ns when the values were balanced. The flexible region A identified by MD simulations comprised residues from W144 to Y168.

HPLC analysis

Identification of products were accomplished by HPLC analysis based on the integration of monomer peaks using external commercial standards. Analysis of the concentration and enantiomeric excess (*e.e.*) of D-HPG was conducted using Agilent 1260 HPLC with Daicel Crownpak CR-I (+) column (150 × 3 mm, 5 μm; Daicel Co., Japan) and pH 1.5 $HClO_4$ a.q./acetonitrile (90/10, v/v) as the mobile phase. Flow: 0.2 ml/min, temperature: 25°C, wavelength: 245 nm.

Directed evolution experiments

Construction of the CgDAPDH variants: Mutant library were conducted by whole plasmid PCR using KOD-Plus-Neo (TOYOBO) and plasmid pET28a-*Cg*DAPDH^{BC621} as template. The primers used in this study are listed in Table A1. The resultant PCR products were digested with DpnI to eliminate the template plasmid. After elimination, 10 μL of digested products were transformed into *E. coli* BL21 (DE3) cells for the following screening or DNA sequencing (GENEWIZ, China).

Cultivation and expression of the mutants in 96-deep-well plates: The single colonies in culture dishes were randomly picked and cultured into 500 μL LB medium with 50 μg mL^{-1} kanamycin in 96-deepwell plates and shaken at 37 °C for 12 h. Then they were 1:10 diluted into 500 μL fresh medium in new 96-deepwell plates (containing 2 g L^{-1} glucose and 4 g L^{-1} lactose). After shaking at 37 °C for 3 h (for cell growth), the temperature was decreased to 25 °C for 15 h (for protein expression). Then the cells were harvested by centrifugation at 3600 ×g at 4 °C for 15 min. The cells were resuspended in 200 μL of the same buffer with 2 mg/mL lysozyme and 0.1% Triton X-100 and the mixture was incubated at 37 °C for 2 h with shaking. Finally, the rude enzyme was obtained by centrifugation at 3600 ×g for 15 min at 4 ^{o}C.

High-throughput screening: After centrifugation, 50 μl supernatant was added into a new 96-well plate containing 500 μl Tris–HCl buffer (50 mM, pH 8.0), 10 mM HPGA and 0.5 mM NADPH and then incubated at 30 ^{o}C for 24 h. After reacting, a same volume of dye mixture (0.01 g L^{-1} of phenazine methosulfate, 0.2 g L^{-1} of nitro blue tetrazolium) was added into the reaction mixture. The mixture was analyzed for activity using a formazan-based method that NADPH reacts with NBT to produce formazan, which could be monitored at 590 nm using BioTek Synergy microplate reader, in the presence of PMS. The absorbance ratios was coupled to the titer of D-HPG and the absorbance at 590 nm for each candidate residue of the site-saturation libraries relative to those of *Cg*DAPDH^{BC621} were calculated. Only when the absorbance of ratio ≤0.8, the strain was sequenced and tested in shaking flasks.

Fermentation medium and conditions

Shaking culture: A single colony of recombinant *E. coli* strain was cultivated overnight (10-12 h, 37 ^{o}C) in LB medium (10 g L^{-1} peptone, 5 g L^{-1} yeast extract, and 10 g L^{-1} NaCl; pH 7.0) with appropriate antibiotics (50 μg ml^{-1} kanamycin or 100 μg ml^{-1} ampicillin) and used as the inoculum (1%). The culture was then transferred into 50 ml Terrific Broth (TB) medium (24 g L^{-1} yeast extract, 12 g L^{-1} tryptone, 5 g L^{-1} glucose,

2.31 g L^{-1} KH_2PO_4, and 16.43 g L^{-1} K_2HPO_4; pH 7.0) containing appropriate antibiotics in a 500 mL flask. When the OD_{600} of the culture broth reached 0.6-0.8, isopropyl β-D-1-thiogalactopyranoside (IPTG) was added to a final concentration of 0.4 mM to induce gene expression. The cells were inducted at 25 °C for 15 h and collected by centrifugation (6000×g, 8 min). Then, the cell pellets were resuspended in an appropriate buffer to the desired density as resting cells for biotransformation.

Fermentor (3 L) culture: Additional larger fermentations were conducted in a 3 L fermentation system (INFORS HT Labfors, Switzerland) with an air flow rate of 1.5 vvm and a stirrer speed of 500 rpm. The pH was maintained at 7.0 by automatically feeding concentrated carbon and nitrogen resources (400 g L^{-1} glucose, 100 g L^{-1} yeast extract, and 25 g L^{-1} tryptone; start feeding after a steep rise in dissolved oxygen, 14 mL h^{-1}). Enzyme expression was induced at 25 °C with 0.4 mM IPTG (final concentration) at an optical density of 4 at 600 nm. Pre-cultures were grown in 500 ml flasks as described above. The cell pellets were collected for preparative biotransformation after 12 h induction.

Enzyme purification

The recombinant *E. coli* strains containing *Pm*L-AAD, *Samb*HmaS, *Pa*MDH, *Cg*DAPDH and *Cg*DAPDH variants were cultured in LB medium containing kanamycin (50 μg mL^{-1}) at 37 °C and 200 rpm. When the culture's optical density (OD_{600}) reached 0.6-0.8, 0.4 mM IPTG (final concentration) was added to induce enzyme expression at 25 ^{o}C for an additional 15 h. The cells were harvested by centrifugation (6000×g, 10 min) at 4 ^{o}C, and resuspended in buffer A (25 mM Tris, 20 mM imidazole, 150 mM NaCl, pH 8.0; 10 ml g^{-1} of wet weight). The cell suspensions were lysed by sonication and centrifuged at 14,000 g for 30 min. The subsequent experiments were performed on an ÄKTA pure system (GE Healthcare) with a HisTrap HP column (5 ml, GE Healthcare). Protein concentration of purified enzyme was measured by detecting absorbance at 280 nm using a NanoDrop 2000c spectrophotometer (Thermo Scientific) and taking into account the calculated extinction coefficients with the ExPASy ProtParam Tool. The purity of proteins were determined by gel filtration and SDS-PAGE. All purification operations were conducted at 4 ^{o}C when necessary.

Kinetic and activity assay

The kinetic parameters of evolved mutants were determined by measuring the initial rates of product formation at different concentrations of HPGA (1-20 mM) in 50 mM Tris-HCl buffer (pH 8.0) at for 30 min at 30 °C. The samples were withdrawn, extracted, and analyzed by HPLC, and KM and kcat then calculated by nonlinear regression according to the Michaelis-Menten equation using Origin software. All the activities were measured in triplicate.

To measure the specific enzyme activities of *Pm*L-AAD, *Samb*HmaS, *Pa*MDH, *Cg*DAPDH and *Cg*DAPDH mutants, the reaction mixture containing 10 mM corresponding substrate and a certain enzyme was

incubated with 50 mM Tris-HCl buffer (pH 8.0) in a final volume of 1 mL at 30 °C for 15 min. The reaction was stopped with centrifugation at 12,000×g for 5 min, samples were analyzed by HPLC. One unit of enzyme is defined as the amount of enzyme producing 1 μmol of corresponding product per minute. The protein concentration was determined by the Bradford protocol, with bovine serum albumin as the standard. All experiments were conducted in triplicate.

Biotransformation procedures in a 3-L bioreactor

The conversion experiments were carried out in a 3-L bioreactor with 800-mL working volume. Recombinant *E. coli* 07 were used as whole-cell biocatalyst (20 g/L) to convert 50 g/L L-tyrosine to D-HPG. The reaction was conducted in 20 mM Tris-HCl buffer (pH 8.5, 0.5 mM $CoSO_4$, 0.7 mM $NADP^+$, and 50 g/L NH_4Cl) at 500 rpm and 30 ^oC for 24 h. At the end of the reaction, 100 μL of supernatant was separated after centrifugation (12000 g, 10 min), diluted with 900 μL mobile phase. The resulting solution was filtered through 0.22 μm membrane filters and analyzed by HPLC for quantifying the products under the conditions stated below.

Results

Cascade design and *in vitro* reconstruction of a D-HPG-biosynthesis pathway

We first compared the structures of L-tyrosine and D-HPG, finding that the L-tyrosine side chain contained one more carbon than the D-HPG side chain, and that the CH_2 subunit at the α position of the L-tyrosine side chain cannot be removed by natural enzymes. Therefore, we designed a sequential cascade to synthesize D-HPG from L-tyrosine (**Fig. 1a**). First, L-tyrosine was deaminized to *p*-hydroxyphenylpyruvate (HPP) by an L-amino acid deaminase (L-AAD; EC 1.4.3.2), followed by HPP transfer to (*S*)-4-hydroxymandelate [(*S*)-HMA] via oxidative decarboxylation by 4-hydroxymandelate synthase (HmaS; EC 1.13.11.46). (*S*)-HMA was subsequently oxidized to HPGA by (*S*)-mandelate dehydrogenase (MDH; EC 1.1.99.31) and finally asymmetrically reduced to D-HPG by DAPDH (**Fig. 1a**).

To reconstruct this cascade pathway *in vitro*, a total of 20 different L-AAD, HmaS, MDH, and DAPDH enzymes from the BRENDA database were evaluated. We subsequently chose an L-AAD from *Proteus mirabilis* (*Pm*L-AAD), HmaS from *Streptomyces ambofaciens* (*Samb*HmaS), MDH from *Pseudomonas aeruginosa* (*Pa*MDH), and a highly stereoselective DAPDH variant from *Corynebacterium glutamicum* (*Cg*DAPDH^{BC621} containing five mutations: R196M/T170I/H245N/Q151L/D155G) according to their specific enzyme activities (Vedha et al. 2006) **(Additional fle 1: Tables S2–S5)**. The selected genes were then amplified, overexpressed, and purified (**Fig. 1b**). To confirm the feasibility of *in vitro* reconstruction, the four enzymes were expressed at a molar ratio of 1:1:1:1 in the presence of 5 mM L-tyrosine. After a 4-h reaction, we confirmed the formation of 0.85 mM D-HPG as the final product by NMR and MS analysis

(**Fig. 1c and Additional fle 1: Fig. S1**), demonstrating the efficacy of the designed cascade using *Pm*L-AAD, *Samb*HmaS, *Pa*MDH, and *Cg*DAPDH^{BC621} for converting L-tyrosine to D-HPG. Furthermore, **Table 2** shows the kinetic parameters of the purified *Pm*L-AAD, *Samb*HmaS, *Pa*MDH, and *Cg*DAPDH^{BC621}. *Pm*L-AAD showed the highest k_{cat}/K_m value (4.48±0.68 $mM^{-1}\cdot min^{-1}$), with the lowest k_{cat}/K_mvalue detected for *Cg*DAPDH^{BC621} (0.009±0.03 $mM^{-1}\cdot min^{-1}$). This result demonstrated *Cg*DAPDH^{BC621} as the rate-limiting step for efficient production of D-HPG.

In vivo construction of the D-HPG biosynthesis pathway

To reconstruct this pathway *in vivo*, the genes encoding *Pm*L-AAD, *Samb*HmaS, *Pa*MDH, and *Cg*DAPDH^{BC621} were inserted into the pACYCDuet-1 and pETDuet-1 plasmids, which were then used to transform into *Escherichia coli* BL21(DE3), resulting in strain *E. coli* 01 (**Fig. 2a**). Following confirmation of enzyme expression (**Fig. 2b)**, we determined the performance of *E. coli* 01 (20 g/L wet cells) at 30 °C, revealing that the D-HPG titer increased from 2.35±0.5 mM to 3.62±0.9 mM along with increasing L-tyrosine concentration (5–15 mM) (**Fig. 2c**); however, at L-tyrosine concentrations >15 mM, the D-HPG titer did not increase. Specifically, the molar conversion of D-HPG decreased from 47.2±0.02% to 14.5±0.2% along with increases in L-tyrosine concentrations from 5 mM to 25 mM. This was due to the accumulation of HPGA, a cascade intermediate, from 1.21±0.2 mM to 11.25±0.8 mM in the conversion broth (**Fig. 2c**). Furthermore, determination of the kinetic parameters of *Pm*L-AAD, *Samb*HmaS, *Pa*MDH, and *Cg*DAPDH^{BC621} in *E. coli* 01 showed that *Pa*MDH exhibited a high k_{cat}/K_m value of 10.71±0.22 $mM^{-1}\cdot min^{-1}$, whereas *Cg*DAPDH^{BC621} continued to show a low k_{cat}/K_m value of 0.23±0.02 $mM^{-1}\cdot min^{-1}$, resulting in a *Pa*MDH:*Cg*DAPDH^{BC621} ratio of 46:1 (**Additional fle 1:Table S6**). This result indicated that the imbalanced catalytic efficiency of the four enzymes promoted accumulation of the intermediate HPGA, which prevented continuous conversion of L-tyrosine to D-HPG.

To control the expression levels of *Pa*MDH and *Cg*DAPDH^{BC621} in strain *E. coli* 01, we selected four promoter sequences with lower activation strengths to replace the T7 promoter in pETDuet-1, resulting in strains *E. coli* 02-06. We found that *E. coli* 02 showed a significantly decreased k_{cat}/K_mvalue for *Pa*MDH (5.32±0.3 $mM^{-1}\cdot min^{-1}$) and an increased k_{cat}/K_mvalue of *Cg*DAPDH^{BC621} (0.59±0.5 $mM^{-1}\cdot min^{-1}$), which was associated with the highest D-HPG titer (4.95±0.5 mM) from 10 mM L-tyrosine but with a low conversion of 49.5±0.02% (**Fig. 2c and 2e**). To increase the expression of *Cg*DAPDH^{BC621}, we employed gene duplication and ribosome-binding sequence regulation; however, this did not increase the D-HPG titer, and HPGA accumulation always higher 4.26±0.04 mM. This was likely due to the low specific activity of *Cg*DAPDH^{BC621} (0.07–0.65 $U\cdot mg^{-1}$ protein), which was unable to continuously transform HPGA into D-HPG.

Increasing *Cg*DAPDH activity by decreasing the $d_{(C6HDAP–C4NNADP)}$ value

As shown in **Fig. 3a**, we elucidated the catalytic mechanism of DAPDH and divided it into three steps: (I) hydride (H^+) transfer from the Cα of *meso*-diaminopimelate (DAP) to the C4N of the $NADP^+$ nicotinamide ring results in formation of an imino acid intermediate, (II) a water molecule subsequently attacks the imino acid intermediate to form a carbinolamine, and (III) *α*-keto acids and ammonia are released from the carbinolamine (Gao et al. 2019). According to this mechanism, we defined two key distances as representing the productive conformation (**Fig. 3b**): the hydride-transfer distance [$d_{(C6HDAP–C4NNADP)}$] describes the distance between the hydrogen atom of DAP and the C4N atom of $NADP^+$, with this used to represent the efficiency of hydride transfer (in step I: 2.3 Å < $d_{(C6HDAP–C4NNADP)}$ < 2.7 Å); and the distance related to water-molecule attack [$d_{(C6DAP–ND1His152)}$] is defined as the distance between the C6 atom of the substrate and the ND1 atom of H152 (in step II: 6.0 Å < $d_{(C6DAP–ND1His154)}$ < 6.8 Å) (Gao et al. 2019). We speculated that the lower specific activity of *Cg*$DAPDH^{BC621}$ was mainly due to $d_{(C6HDAP–C4NNADP)}$ or $d_{(C6DAP–ND1His154)}$ being outside of the range required for optimal DAPDH catalysis.

A homology model of *Cg*$DAPDH^{BC621}$ was reconstructed using SWISS-MODEL (https://swissmodel.expasy.org/) based on the crystal structure of *Cg*DAPDH (PDB ID: 5LOA) (Parmeggiani et al. 2016). Docking analysis performed using the *Cg*$DAPDH^{BC621}$ structural model and D-HPG (**Fig. 3c**) revealed the following: 1) the α6-helix region of *Cg*$DAPDH^{BC621}$ (residues R158–L149) resides in close proximity to the carbonyl group of D-HPG, W119 and W144 sterically hinder the benzene ring of D-HPG, and W144, H152, I169, and Y223 surround the phenolic hydroxyl group of D-HPG; 2) additionally, in the *Cg*$DAPDH^{BC621}$ active site, we identified four hydrogen bonds between D-HPG with D120, L150, G151, and N270, as well as a pi-pi stacking interaction between D-HPG with the pyrrole ring of W144, anchoring D-HPG in the binding cavity. In this conformation, the $d_{(C6HDAP–C4NNADP)}$ is 3.5 Å, which is higher than the suitable hydride-transfer distance (range: 2.3–2.7 Å). These findings indicated that D-HPG incompletely fit in the binding cavity, and the position is not beneficial to hydride transfer. Therefore, the substrate-binding cavity of *Cg*$DAPDH^{BC621}$ required alteration to rotate the D-HPG conformation to decrease $d_{(C6HDAP–C4NNADP)}$.

To reshape the substrate-binding cavity of *Cg*$DAPDH^{BC621}$, we employed a “conformation rotation” strategy targeting nine candidate residues (W119, D120, W144, L150, G151, H152, I169, N270, and Y223) for NNK site-saturation mutagenesis. To efficiently screen potential positive variants, we developed a formazan-based high-throughput method that coupled D-HPG titer with the absorbance at 590 nm. The lowest absorbance ratios for each mutated candidate residue relative to its variant in *Cg*$DAPDH^{BC621}$ are shown in **Additional fle 1: Table S7**. To rule out detection errors, we only selected and sequenced variants with absorbance ratios ≤0.8. We ultimately identified four variants (*Cg*$DAPDH^{BC621/I169P}$, *Cg*$DAPDH^{BC621/I169Y}$, *Cg*$DAPDH^{BC621/D120S}$, and *Cg*$DAPDH^{BC621/Y223C}$), with *Cg*$DAPDH^{BC621/I169P}$

showing a 2.3-fold increase in specific activity (0.32±0.58 U·mg^{-1} protein) relative to *Cg*DAPDH^{BC621} (**Additional fle 1: Fig. S3**). To further increase this activity, we constructed a recombinant variant library that included four double-mutant variants (*Cg*DAPDH$^{BC621/D120S/I169P}$, *Cg*DAPDH$^{BC621/I169P/Y223C}$, *Cg*DAPDH$^{BC621/D120S/I169Y}$, and *Cg*DAPDH$^{BC621/I169Y/Y223C}$). The results showed that *Cg*DAPDH$^{BC621/D120S/I169P}$ presented a 5.3-fold increase in activity (0.74±0.21 U·mg^{-1} protein) relative to *Cg*DAPDH^{BC621} (**Additional fle 1: Fig. S4**). On the other hand, an iterative saturation variant library based on *Cg*DAPDH$^{BC621/I169P}$ variant was constructed, in which *Cg*DAPDH$^{BC621/W144S/I169P}$ revealed a 6.2-fold increase in activity relative to *Cg*DAPDH^{BC621} (**Additional fle 1: Fig. S5**). Furthermore, combining variants *Cg*DAPDH$^{BC621/D120S/I169P}$ and *Cg*DAPDH$^{BC621/W144S/I169P}$ to obtain *Cg*DAPDH$^{BC621/D120S/W144S/I169P}$ resulted in a specific activity of 5.32±0.85 U·mg^{-1} protein, which was 38-fold higher than that of *Cg*DAPDH^{BC621} (**Fig. 4a**).

Structural comparison of *Cg*DAPDH^{BC621} with *Cg*DAPDH$^{BC621/D120S/W144S/I169P}$ (**Fig. 4b and 4c**) revealed the following: 1) the I169P and W144S mutations increased the area for accommodating the phenol group of D-HPG, thereby providing D-HPG with a space for “conformational rotation”; 2) the D120S mutation resulted in a decreased hydrogen bond length with the amino group of D-HPG (from 3.0 Å to 2.9 Å), which decreased the distance between L150 and the D-HPG carboxyl group (from 3.3 Å to 3.1 Å) (**Additional fle 1: Fig. S6**), and the W144S mutation eliminated the pi-pi stacking interaction between W144 and D-HPG (**Fig. 4d**). These modifications decreased the $d_{(C6HDAP-C4NNADP)}$ value from 3.5 Å to 2.7 Å while also increasing the conformational stability of *Cg*DAPDH$^{BC621/D120S/W144S/I169P}$ relative to *Cg*DAPDH^{BC621} (a decrease in RMSD from 3.07 Å to 2.80 Å) and decreasing the flexibility of residues in region A (W144–Y168) (**Fig. 4f and 4g**). As a result, the K_m value of *Cg*DAPDH$^{BC621/D120S/W144S/I169P}$ (2.48±0.28 mM) was 8.21-fold lower and the k_{cat} value (2.69±0.30 min^{-1}) was 14.16-fold higher than those of *Cg*DAPDH^{BC621} (K_m=20.37±0.19 mM and k_{cat} =0.19±0.37 min^{-1}, respectively). This resulted in a 120-fold increase in the k_{cat}/K_m value of *Cg*DAPDH$^{BC621/D120S/W144S/I169P}$ (1.08 mM^{-1}·min^{-1}) relative to that of *Cg*DAPDH^{BC621} (**Table 3**).

One-pot production of D-HPG at the 3-L scale

We used *Cg*DAPDH$^{BC621/D120S/W144S/I169P}$ to replace *Cg*DAPDH^{BC621} in *E. coli* 02, resulting in *E. coli* 07 (**Additional fle 1: Fig. S7**). After 24 h, we found that the D-HPG titer increased to 9.03±0.32 mM along with a 90.3±0.03% molar conversion, which was a 1.82-fold increase relative to *E. coli* 02. Additionally, HPGA accumulation remained <0.22±0.06 mM, indicating that the catalytic efficiency of *Cg*DAPDH$^{BC621/D120S/W144S/I169P}$ matched that of *Pa*MDH.

We then evaluated the effect of inducers (IPTG and lactose) on specific activity and cell growth (**Fig. 5a).** The results showed that induction with IPTG (0.4 mM IPTG at 2 h) resulted in a 1.19-fold increase in specific activity for *Cg*DAPDH$^{BC621/D120S/W144S/I169P}$ (5.42±1.2 U·mg^{-1}) and a 1.53-fold increase in cell

growth (OD_{600}=50.1±1.4) relative to lactose induction. Additionally, for the same IPTG concentration and induction time, we determined the specific activities for *Pm*L-AAD, *Samb*HmaS, and *Pa*MDH at 12.5±1.2 $U{\cdot}mg^{-1}$, 10.3±0.9 $U{\cdot}mg^{-1}$, and 15.6±1.5 $U{\cdot}mg^{-1}$, respectively. Moreover, increase in the induction time from 2 h to 15 h resulted in the highest *Cg*DAPDH$^{BC621/D120S/W144S/I169P}$ activity (6.02±0.6 $U{\cdot}mg^{-1}$), although this decreased at times >15 h (**Fig. 5b**). Furthermore, for 15-h induction by 0.4 mM IPTG, *Cg*DAPDH$^{BC621/D120S/W144S/I169P}$ specific activity was further increased to 6.14±0.5 $U{\cdot}mg^{-1}$ at a temperature increased from 16 °C to 25 °C, with increased cell growth also observed under these conditions [OD_{600}=20.4±0.1 (16 °C) vs. 41.5±1.2 (25 °C)] (**Fig. 5c**). These results identified the optimal conditions as 15-h induction by IPTG at 25 °C after culturing at 37 °C for 2 h.

We then investigated the effects of buffer type, pH, and temperature on the D-HPG titer at the 3-L scale. As shown in **Fig. 5d**, a higher D-HPG titer was detected (39.23±1.2 g/L) in Tris-HCl buffer higher than that of other three buffers. In Tris-HCl buffer, the D-HPG titer was further increased to a peak of 40.17±0.9 g/L within a pH range of 6.0 to 8.5 (**Fig. 5e**). Assessment of the transformation temperature (range: 25–35 °C) revealed a high D-HPG titer (40.31±1.1 g/L) and conversion (87.38±0.6 %) at 30 °C (**Fig. 5f**).

Under the optimal induction and transformation conditions [0.7 mM $NADP^+$, 0.5 mM $CoSO_4$, 20 mM Tris-HCl buffer (pH 8.5) and 30 °C], we obtained 42.69 g/L D-HPG in a 3-L fermentation using 20 g/L (wet cell) *E. coli* 07 from 50 g/L L-tyrosine in 20 h with a 92.5% conversion and >99% *ee*.

Discussion

Numerous methods have been designed to efficiently produce D-HPG, with these mainly including chemical synthesis and enzymatic conversion. Chemical synthesis includes chiral separation, esterification-coupled hydrolysis, induced crystallization, and asymmetric transformation (Yu et al. 2009; Zhang et al. 2010). Although these methods are efficient for D-HPG production, their disadvantages include the need for high-cost precursors, multi-step separation and purification processes, and the production of toxic intermediates (Van et al. 2007; Zhang et al. 2015). For enzymatic conversion, a recent study used DL-HPH as a substrate in a two-step enzymatic process catalyzed by Hase and Case, resulting in 29.10 g/L D-HPG produced from 30 g/L DL-HPH in 12 h (Hu and Lin 2015); however, DL-HPH is usually obtained by the condensation of urea, phenol, and glyoxylic acid, which requires harsh conditions, thereby increasing the cost of D-HPG production (Bellini et al. 2019). Therefore, the development of a lower-cost and environmentally friendly method for efficient production of D-HPG remains a necessity. In this study, we designed a novel cascade pathway for the production of D-HPG from L-tyrosine, a low-cost and widely available amino acid. This pathway has three advantages: 1) use of a low-cost substrate and reagents (L-tyrosine and NH_4Cl, respectively) to produce D-HPG; 2) simple procedures using a single *E. coli* strain 07 for one-pot L-tyrosine conversion to D-HPG and no additional separation/purification processes; and 3) an environmentally friendly process with no generation of toxic intermediates (those generated *in situ* can be directly consumed in the reaction sequence).

We found high levels of the intermediate HPGA generated during conversion (4.26 ± 0.04 mM) due to the lower activity of *Cg*DAPDH^{BC621}, which caused an imbalance in enzyme activity in the cascade. Therefore, we applied a mechanism-guided "conformation rotation" strategy to shorten the $d_{(C6HDAP-C4NNADP)}$ in variant *Cg*DAPDH$^{BC621/D120S/W144S/I169P}$, resulting in 38-fold and 120-fold increases in the specific activity and k_{cat}/K_m value relative to *Cg*DAPDH^{BC621}, respectively. To improve the catalytic properties of DAPDH, previous studies employed several protein engineering strategies, including random mutagenesis and rational design (Akita et al. 2018; Cheng et al. 2018; Zhang et al. 2018). Random mutagenesis can optimize enzyme efficiency without the need for a detailed knowledge of protein structure (Cho et al. 2019). *Cg*DAPDH^{BC621} was originally obtained after screening ~ 100,000 variants and exhibited a 975-fold increase in specific activity toward D-2-aminooctanoate (Vedha et al. 2006). However, random mutation might not cover all sequences and requires an enormous screening effort (Chen et al. 2019). In contrast, rational design is based on analysis of structure–function relationships or catalytic mechanisms and greatly reduces screening efforts (Kan et al. 2016). Recently, this approach was used to identify a double-mutant variant of *Symbiobacterium thermophilum St*DAPDH$^{W121L/H227I}$ via structural alignment, resulting in a 34.45-fold increase in activity toward 2-oxo-4-phenylbutyric acid relative to wild-type *St*DAPDH (Cheng et al. 2018). However, existing rational-design strategies mainly focus on the DAPDH active site, with few strategies addressing the asymmetric amination mechanism of the DAPDH. In this study, our use of the "conformation rotation" strategy had three main characteristics: 1) define the rate-limiting step based on the reaction mechanism (the hydride-transfer distance [$d_{(C6HDAP-C4NNADP)}$]) (Fig. 3a) and make appropriate changes to promote efficient asymmetric amination of HPGA; 2) identify hotspots, which were defined in this case as bulky residues proximal to the D-HPG substrate, and use them to perform rational engineering of beneficial variants; and 3) create a small mutation library comprising multiple variants for high-throughput screening, which was more efficient than random mutagenesis and enabled rapid identification of optimal variants.

By introducing *Cg*DAPDH$^{BC621/D120S/W144S/I169P}$ into strain *E. coli* 07 and then optimizing the induction and transformation conditions, we obtained 42.69 g/L of D-HPG with a 92.5% conversion and > 99% *ee* during one-pot transformation. To the best of our knowledge, this represents the highest reported D-HPG titer. These findings demonstrate the efficacy of the developed cascade pathway for improving the D-HPG titer and represent a potentially attractive strategy for use in industrial production of D-HPG.

Conclusions

To develop an efficient method for D-HPG production, we designed a novel four-enzyme cascade pathway using L-tyrosine as substrate and reconstructed this pathway *in vivo*. We further increased the efficiency of the pathway by improving the catalytic efficiency of *Cg*DAPDH, the rate-limiting step, toward the HPGA intermediate using a mechanism-guided "conformation rotation" strategy. Introduction of the best engineered variant (*Cg*DAPDH$^{BC621/D120S/W144S/I169P}$) into *E. coli* 07 allowed one-pot conversion of L-tyrosine to 42.69 g/L D-HPG during 3-L fermentation. These results describe a potential enzymatic process that allows industrial-scale production of D-HPG from cheap amino acids.

Abbreviations

D-HPG, D-*p*-hydroxyphenylglycine; HPGA, 4-hydroxyphenylglyoxylic acid; DL-HPG, DL-*p*-hydroxyphenylglycine; DL-HPH, DL-hydroxyphenylhydantoin; DAPDH, *meso*- diaminopimelate dehydrogenase; HPP, *p*-hydroxyphenylpyruvate; L-AAD, L-amino acid deaminase; (*S*)-HMA, (*S*)-4-hydroxymandelate; HmaS, 4-hydroxymandelate synthase; MDH, (*S*)-mandelate dehydrogenase.

Declarations

Ethics approval and consent to participate

Not applicable.

Consent for publication

All authors approved the consent for publishing the manuscript to bioresources and bioprocessing.

Availability of data and materials

All data generated or analyzed during this study are included in this article.

Competing interests

The authors declare that they have no competing interests.

Funding

This work was financially supported by the Provincial Natural Science Foundation of Jiangsu Province (BK20200622), the Youth Program of National Natural Science Foundation of China (22008089), the General Program of National Natural Science Foundation of China (21878126), the Key Technologies R & D Program of Jiangsu Province (BE2018623), and the National First-Class Discipline Program of Light Industry Technology and Engineering (LITE2018-20).

Authors' contributions

XT and SZ conceived the study. XT and WS made contributions to the design of the experiments, the acquisition of data, the analysis and interpretation of data and contributed to the manuscript writing. JL, CG, XLC, LML and JW conceived and organized the study and helped to draft the manuscript, and have revised the manuscript. All authors read and approved the final manuscript.

Acknowledgements

Not applicable.

References

Ahmed S T, Parmeggiani F, Weise N J, Flitsch S L, Turner N J (2015) Chemoenzymatic synthesis of optically pure L- and D-biarylalanines through biocatalytic asymmetric amination and palladium-catalyzed arylation. ACS Catal 5(9): 5410-5413. https://10.1021/acscatal.5b01132

Akita H, Doi K, Kawarabayasi Y, Ohshima T (2012) Creation of a thermostable NADP(+)-dependent D-amino acid dehydrogenase from *Ureibacillus thermosphaericus* strain A1 *meso*-diaminopimelate dehydrogenase by site-directed mutagenesis. Biotechnol Lett 34(9): 1693-1699. https://10.1007/s10529-012-0952-1

Akita H, Hayashi J, Sakuraba H, Ohshima T (2018) Artificial thermostable D-amino acid dehydrogenase: creation and application. Front Microbiol 9: 11. https://10.3389/fmicb.2018.01760

Aranaz I, Acosta N, Fernandez V M E, Heras A (2015) Optimization of D-amino acid production catalyzed by immobilized multi-enzyme system in polyelectrolyte complex gel capsules. J Mol Catal B: Enzym 121: 45-52. https://10.1016/j.molcatb.2015.06.003

Bellini R G, Coronado M A, Paschoal A R, do Rego T G, Hungria M, Ribeiro d V, Ana Tereza, Nicolas M F (2019) Structural analysis of a novel N-carbamoyl-D-amino acid amidohydrolase from a Brazilian *Bradyrhizobium japonicum* strain: *in silico* insights by molecular modelling, docking and molecular dynamics. J Mol Graphics Modell 86: 35-42. https://10.1016/j.jmgm.2018.10.005

Chen X, Zhang H L, Maria S, M. A., Liu W D, Li J, Feng J H, Liu X T, Osuna S, Guo R T, Wu Q Q, Zhu D M, Ma Y H (2019) Efficient reductive desymmetrization of bulky 1,3-cyclodiketones enabled by structure-guided directed evolution of a carbonyl reductase. Nat Catal 2(10): 931-941. https://10.1038/s41929-019-0347-y

Cheng X, Chen X, Feng J, Wu Q, Zhu D (2018) Structure-guided engineering of *meso*-diaminopimelate dehydrogenase for enantioselective reductive amination of sterically bulky 2-keto acids. Catal Sci Technol 8(19): 4994-5002. https://10.1039/c8cy01426d

Cho I, Prier C K, Jia Z J, Zhang R K, Gorbe T, Arnold F H (2019) Enantioselective aminohydroxylation of styrenyl olefins catalyzed by an engineered hemoprotein. Angew Chem Int Ed Engl. https://10.1002/anie.201812968

Diez V, Loznik M, Taylor S, Winn M, Rattray N J W, Podmore H, Micklefield J, Goodacre R, Medema M H, Mueller U, Bovenberg R, Janssen D B, Takano E (2015) Functional exchangeability of oxidase and dehydrogenase reactions in the biosynthesis of hydroxyphenylglycine, a nonribosomal peptide building block. ACS Synth Biol 4(7): 796-807. https://10.1021/sb500368w

Gao X, Chen X, Liu W, Feng J, Wu Q, Hua L, Zhu D (2012) A novel *meso*-diaminopimelate dehydrogenase from *Symbiobacterium thermophilum*: overexpression, characterization, and potential for D-amino acid synthesis. Appl Environ Microbiol 78(24): 8595-8600. https://10.1128/aem.02234-12

Gao X, Huang F, Feng J, Chen X, Zhang H J, Wang Z, Wu Q, Zhu D M (2013) Engineering the *meso*-diaminopimelate dehydrogenase from *Symbiobacterium thermophilum* by site saturation mutagenesis for D-phenylalanine synthesis. Appl Environ Microbiol 79(16): 5078-5081. https://10.1128/aem.01049-13

Gao X, Ma Q, Chen M, Dong M M, Pu Z J, Zhang X H, Song Y D (2019) Insight into the highly conserved and differentiated co-factor binding sites of *meso*-diaminopimelate dehydrogenase *St*DAPDH. J Chem Inf Model 59(5): 2331-2338. https://10.1021/acs.jcim.8b00879

Gao X, Zhang Z, Zhang Y, Li Y, Zhu H, Wang S, Li C (2017) A newly determined member of the *meso*-diaminopimelate dehydrogenase family with a broad substrate spectrum. Appl Environ Microbiol 83(11): e00476-00417 https://10.1128/AEM.00476-17

Hayashi J, Seto T, Akita H, Watanabe M, Hoshino T, Yoneda K, Ohshima T, Sakuraba H (2017) Structure-based engineering of an artificially generated NADP(+)-dependent D-amino acid dehydrogenase. Appl Environ Microbiol 83(11). https://10.1128/aem.00491-17

Hu X, Lin B (2015) Efficient production of D-HPG with an immobilized transgenic strain *E. coli* LY13-05. Biotechnol Biotechnol Equip 29(5): 1003-1010. https://10.1080/13102818.2015.1044909

Kan S B J, Lewis R D, Chen K, Arnold F H (2016) Directed evolution of cytochrome c for carbon-silicon bond formation: bringing silicon to life. Science 354(6315): 1048-1051. https://10.1126/science.aah6219

Liu W, Guo R T, Chen X, Li Z, Gao X, Huang C, Wu Q, Feng J, Zhu D (2015) Structural analysis reveals the substrate-binding mechanism for the expanded substrate specificity of mutant *meso*-diaminopimelate dehydrogenase. Chembiochem 16(6): 924-929. https://10.1002/cbic.201402632

Liu W, Li Z, Huang C H, Guo R T, Zhao L M, Zhang D L, Chen X, Wu Q Q, Zhu D M (2014) Structural and mutational studies on the unusual substrate specificity of *meso*-diaminopimelate dehydrogenase from *Symbiobacterium thermophilum*. Chembiochem 15(2): 217-222. https://10.1002/cbic.201300691

Liu Y, Zhu L, Qi W, Yu B (2019) Biocatalytic production of D-*p*-hydroxyphenylglycine by optimizing protein expression and cell wall engineering in *Escherichia coli*. Appl Microbiol Biotechnol 103(21-22): 8839-8851. https://10.1007/s00253-019-10155-z

Nandanwar H S, Prajapati R, Hoondal G S (2013) (D)-*p*-hydroxyphenylglycine production by thermostable D-hydantoinase from *Brevibacillus parabrevis*-PHG1. Biocatal Biotransform 31(1): 22-32. https://10.3109/10242422.2012.755962

Parmeggiani F, Ahmed S T, Thompson M P, Weise N J, Galman J L, Gahloth D, Dunstan M S, Leys D, Turner N J (2016) Single-biocatalyst synthesis of enantiopure D-arylalanines exploiting an engineered D-

amino acid dehydrogenase. Adv Synth Catal 358(20): 3298-3306. https://10.1002/adsc.201600682

Pollegioni L, Rosini E, Molla G (2020) Advances in enzymatic synthesis of D-amino acids. Int J Mol Sci 21(9). https://10.3390/ijms21093206

Tripathi C K M, Bihari V, Tyagi R D (2000) Microbial production of D-amino acids. Process Biochem 35(10): 1247-1251. https://10.1016/s0032-9592(00)00170-9

Van L, Steven G., Oh T J, Liu W, Wendt P, Evelyn, Shen B (2007) Characterization of the maduropeptin biosynthetic gene cluster from *Actinomadura madurae* ATCC 39144 supporting a unifying paradigm for enediyne biosynthesis. J Am Chem Soc 129(43): 13082-13094. https://10.1021/ja073275o

Vedha P, K., Gunawardana M, Rozzell J D, Novick S J (2006) Creation of a broad-range and highly stereoselective D-amino acid dehydrogenase for the one-step synthesis of D-amino acids. J Am Chem Soc 128(33): 10923-10929. https://10.1021/ja0603960

Yu H, Yang S, Jiang W, Yang Y (2009) Efficient biocatalytic production of D-4-hydroxyphenylglycine by whole cells of recombinant *Ralstonia pickettii*. Folia Microbiol 54(6): 509-515. https://10.1007/s12223-009-0073-y

Zhang D, Zhu F, Fan W, Tao R, Yu H, Yang Y, Jiang W, Yang S (2011) Gradually accumulating beneficial mutations to improve the thermostability of N-carbamoyl-D-amino acid amidohydrolase by step-wise evolution. Appl Microbiol Biotechnol 90(4): 1361-1371. https://10.1007/s00253-011-3114-9

Zhang J, Cai Z (2014) Efficient and cost-effective production of D-*p*-hydroxyphenylglycine by whole-cell bioconversion. Biotechnol Bioprocess Eng 19(1): 76-82. https://10.1007/s12257-013-0451-9

Zhang P, Luo J, Tang K, Yi J, Yang C (2015) Kinetics study on reactive extraction of D-*p*-hydroxyphenylglycine by BINAP-palladium complex in Lewis cell. Chem Eng Process Intensification 93: 50-55. https://10.1016/j.cep.2015.04.007

Zhang Y, Liu R, Xu X (2010) One-pot, two-step enzymatic synthesis of amoxicillin by complexing with Zn^{2+}. Appl Microbiol Biotechnol 88(1): 49-55. https://10.1007/s00253-010-2727-8

Zhang Y, Ma Q, Dong M, Zhang X, Chen Y, Gao X, Song Y (2018) Essential role of amino acid position 71 in substrate preference by *meso*-diaminopimelate dehydrogenase from *Symbiobacterium thermophilum* IAM14863. Enzyme Microb Technol 111: 57-62. https://10.1016/j.enzmictec.2018.01.001

Zhao Y, Xu L B (2015) Chiral separation of hydroxyphenylglycine by ligand exchange micellar electrokinetic capillary chromatography. Chromatographia 78(9-10): 717-721. https://10.1007/s10337-015-2873-3

Tables

Table 1 Host strains and plasmids used in this study

Strain[a]	Recombinant plasmids[b] in the strain
E. coli 01	pACYC-*Pm*L-AAD-*Samb*HmaS, pET-*Pa*MDH-*Cg*DAPDH^{BC621}
E. coli 02	pET-$_{(Tac)}$*Pa*MDH-*Cg*DAPDH^{BC621}
E. coli 03	pET-$_{(T5)}$*Pa*MDH-*Cg*DAPDH^{BC621}
E. coli 04	pET-$_{(Tre)}$*Pa*MDH-*Cg*DAPDH^{BC621}
E. coli 05	pET-$_{(Trp)}$*Pa*MDH-*Cg*DAPDH^{BC621}
E. coli 06	pET-$_{(T7)}$*Pa*MDH-*Cg*DAPDH^{BC621}
E. coli 07	pACYC-*Pm*L-AAD-*Samb*HmaS, pET-$_{(Tac)}$*Pa*MDH-*Cg*DAPDH$^{BC621/D120S/W144S/I169P}$

Note. L-AAD: L-amino acid deaminase; HmaS: 4-hydroxymandelate synthase; MDH: (*S*)-mandelate dehydrogenase; DAPDH: *meso*-diaminopimelate dehydrogenase.

[a] The strains were constructed by transforming the corresponding recombinant plasmids into *E. coli* BL21 (DE3) express strains (New England Biolabs).

[b] The recombinant plasmids were constructed on pACYCDuet-1 or pETDuet-1 (Novagen).

Table 2 Kinetic constants of purified *Pm*L-AAD, *Samb*HmaS, *Pa*MDH, *Cg*DAPDH^{BC621}

Enzyme	Specific activity[a] (U·mg^{-1} protein)	K_m (mM)	k_{cat} (min^{-1})	k_{cat}/K_m[b] (mM^{-1}·min^{-1})
*Pm*L-AAD	8.95±0.38	1.29±0.18	5.78±0.07	4.48±0.68
*Samb*HmaS	7.25±0.98	2.37±0.04	6.44±0.25	2.72±0.13
*Pa*MDH	9.26±0.37	3.92±0.27	10.11±0.18	2.58±0.21
*Cg*DAPDH^{BC621}	0.14±1.60	20.37±1.08	0.19±0.47	0.009±0.03

Note. L-AAD: L-amino acid deaminase; HmaS: 4-hydroxymandelate synthase; MDH: (*S*)-mandelate dehydrogenase; DAPDH: *meso*-diaminopimelate dehydrogenase.

[a] The specific activity was determined with 10 μM purified enzymes and 10 mM corresponding substrate in 1ml Tris-HCl buffer (50 mM, pH 8.0) at 30 ^{o}C for 15 min.

[b] The k_{cat}/K_m values was determined with 10 μM purified enzymes and 1-20 mM corresponding substrate in 1ml Tris-HCl buffer (50 mM, pH 8.0) at 30 ^{o}C for 30 min.

Table 3 Kinetic constants of purified *Cg*DAPDH^{BC621} and its variants

Variants	Specific activity[a] (U·mg^{-1} protein)	K_m (mM)	k_{cat} (min^{-1})	k_{cat}/K_m[b] (mM^{-1}·min^{-1})
BC621	0.14±0.18	20.37±0.19	0.19±0.37	0.009
I169P	0.32±0.58	8.17±0.89	1.48±0.25	0.18
D120S/I169P	0.74±0.21	7.83±0.03	1.46±0.70	0.19
W144S/I169P	0.87±0.47	8.07±0.68	1.35±1.39	0.17
D120S/W144S/I169P	5.32±0.85	2.48±0.28	2.69±0.30	1.08

Note. DAPDH: *meso*-diaminopimelate dehydrogenase.

[a] The specific activity was determined with 10 μM purified *Cg*DAPDH^{BC621} or its variants and 10 mM HPGA in 1ml Tris-HCl buffer (50 mM, pH 8.0, 20 mM NH_4Cl) at 30 ^{o}C for 15 min.

[b] The k_{cat}/K_m values was determined with 10 μM purified *Cg*DAPDH^{BC621} or its variants and 1-20 mM HPGA in 1ml Tris-HCl buffer (50 mM, pH 8.0, 10 mM NH_4Cl) at 30 ^{o}C for 30 min.

Figures

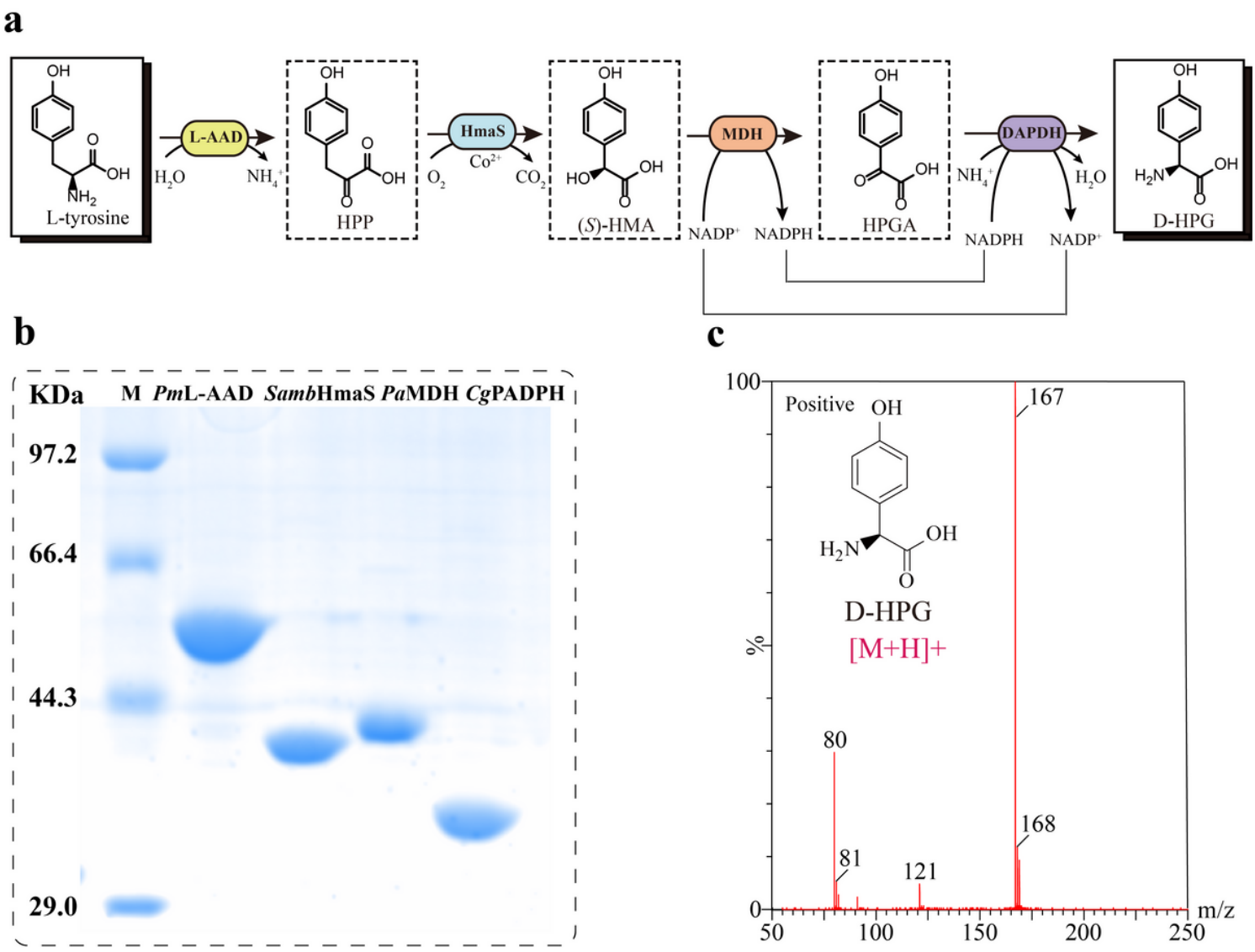

Figure 1

Cascade design and in vitro reconstruction of D-HPG biosynthesis pathway. (a) Schematic representation of D-HPG biosynthesis from L-tyrosine through a four-enzyme cascade. (b) Cascade pathway protein characterization. Enzymes involved in this system were purified and analyzed by SDS-PAGE. (c) Analysis of the in vitro reconstructed system with LC–MS. The four-enzyme system was supplemented with 10 mM L-tyrosine, 0.5 mM NADP+, 20 mM NH4Cl, 0.5 mM CoSO4, and each of the four purified enzymes with 10 μM.

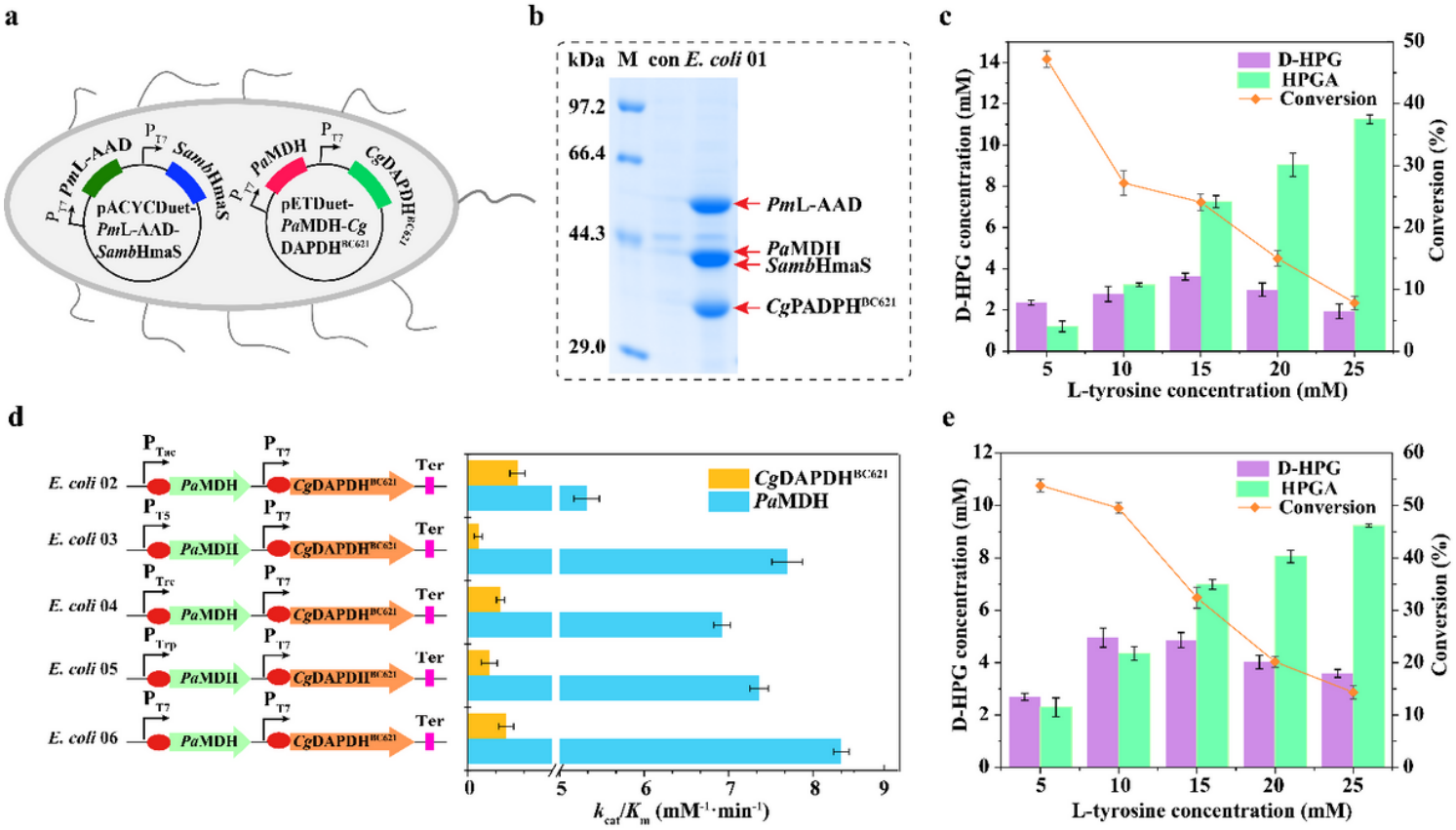

Figure 2

In vivo construction and optimization of multi-step cascade reactions. (a) Strain E. coli 01 containing double plasmids to express PmL-AAD, SambHmaS, PaMDH, and CgDAPDHBC621. (b) SDS-PAGE analysis of strain E. coli 01 from cell-free extracts. M: Maker; con: E. coli BL21 without overexpressing any enzymes. (c) Effect of substrate loading on D-HPG production by strain E. coli 01. (d) The kcat/Km of PaMDH and CgDAPDHBC621 in recombinant strains with different promoter sequences. (e) Effect of substrate loading on D-HPG production by strain E. coli 02. The reactions were supplemented with varying concentrations of L-tyrosine from 5 to 25 mM and 20 g/L wet cell added at 30 oC. The conversion and titer were obtained after completion of the reactions and determined by HPLC analysis. The values are averages of three experiments.

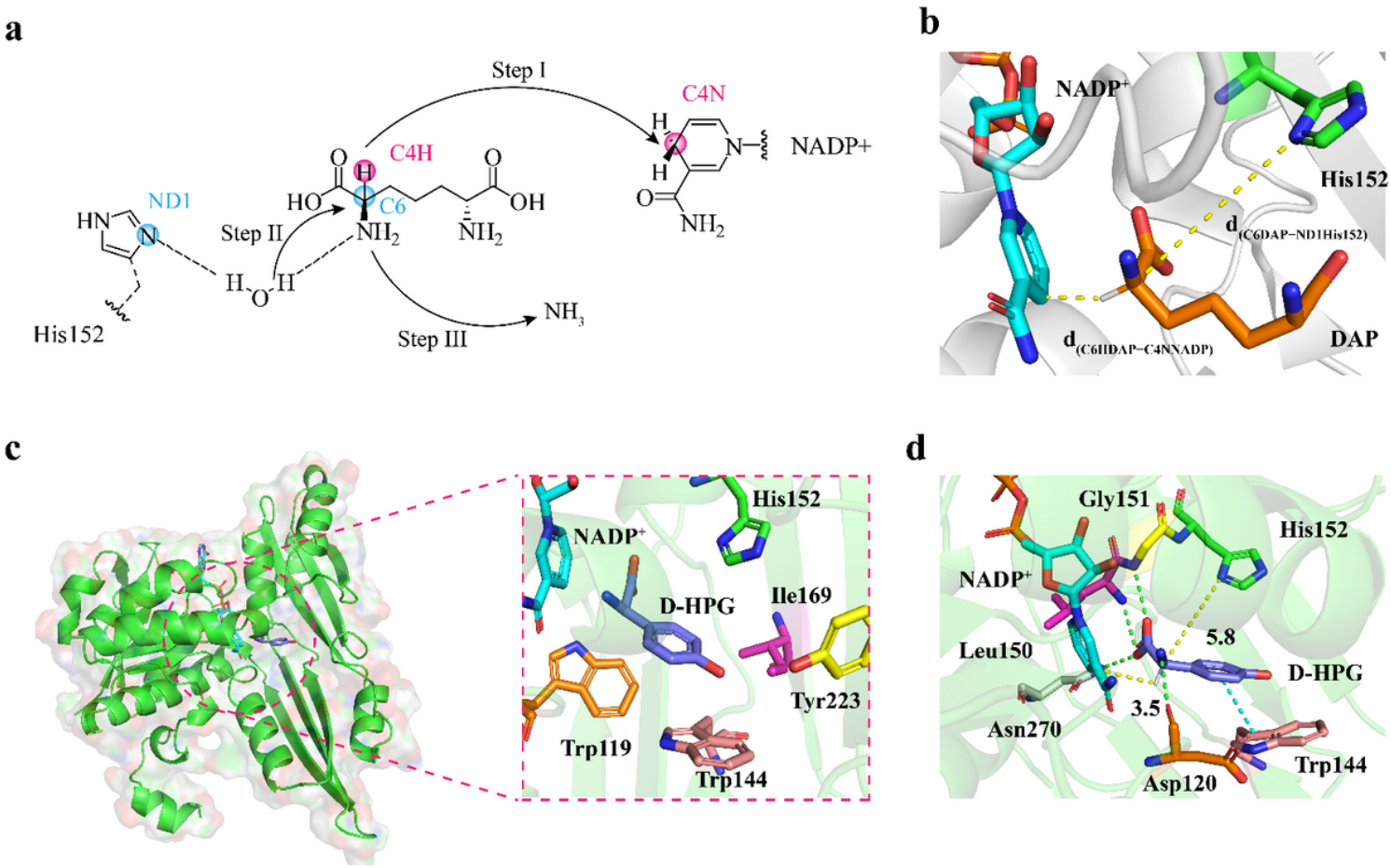

Figure 3

Putative mechanism of DAPDH catalysis and docking analysis of CgDAPDHBC621-NADP+ with D-HPG. (a) A schematic view of the DAPDH reduction mechanism adapted to DAP. the hydride transfer from DAP (C4H) to NADP+ (C4N) are marked as pink spheres, the C6 of imino acid intermediate attacked by water and the ND1 of H152 are marked as blue spheres. (b) Two key distances in reductive amination process. The yellow dash lines denote d(C6HDAP−C4NNADP) and d(C6DAP−ND1His152), respectively. NADP+ cofactor is shown in cyan, DAP is shown in orange, and residue H152 is shown in green. (c) A detailed active site view of CgDAPDHBC621-NADP+ with D-HPG. D-HPG is shown in purple, residue W119 is shown in orange, W144 is shown in lightpink, I169 is shown in magenta, and Y223 is shown in yellow. (d) The interactions between D-HPG and CgDAPDHBC621 and the two key distance values. The green dash lines denote hydrogen-bond interactions and the cyan dash line denote pi-pi stacking interaction. Residue D120 is shown in orange, L150 is shown in magenta, G151 is shown in yellow, and N270 is shown in white.

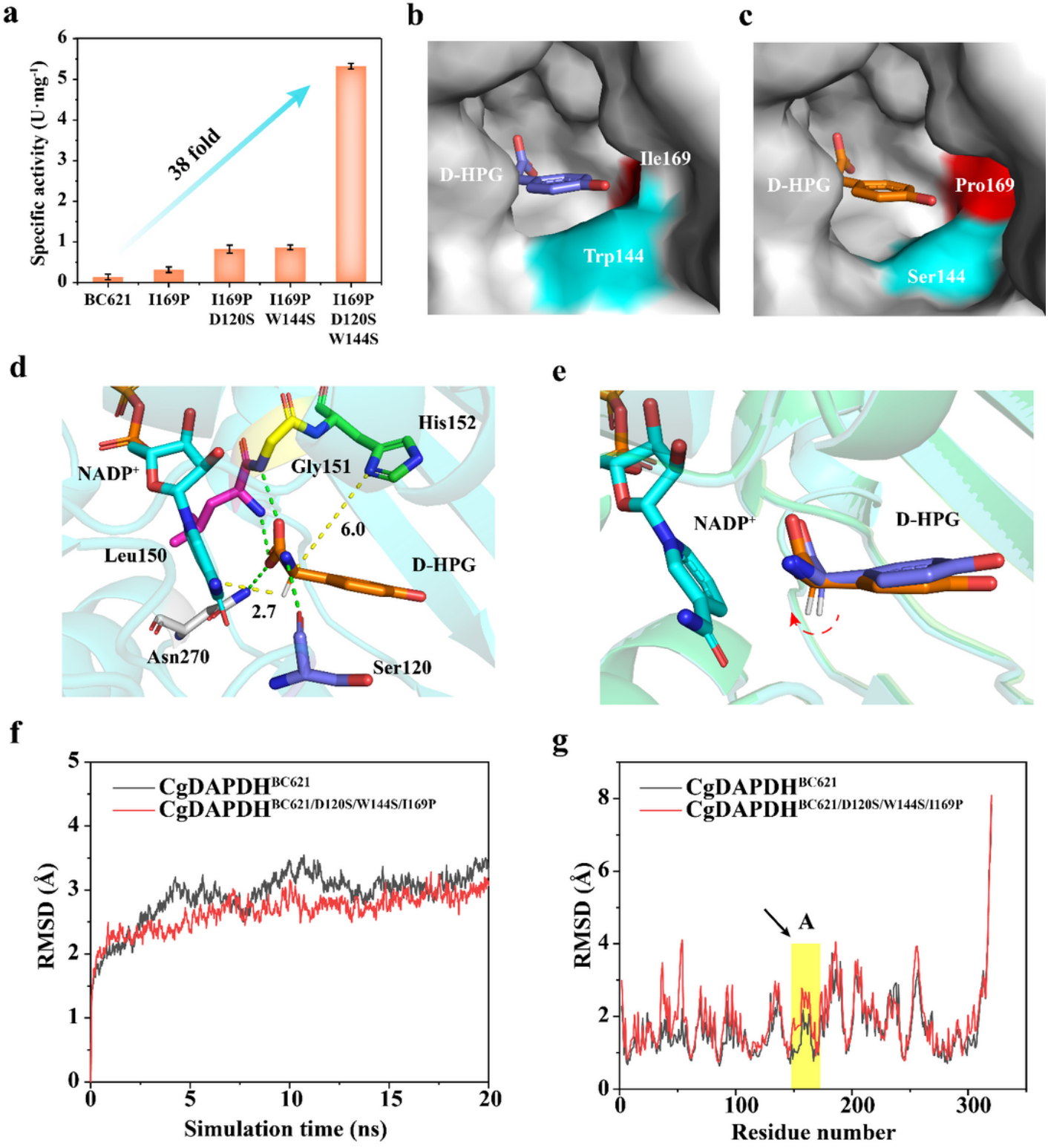

Figure 4

Improvement of the catalytic activity of CgDAPDHBC621 toward HPGA by “conformational rotation” strategy. (a) Directed evolution of the parent CgDAPDHBC621 for reductive amination of HPGA. (b) The binding pocket surface of CgDAPDHBC621. D-HPG is shown in purple. (c) The binding pocket surface of CgDAPDHBC621/D120S/W144S/I169P. D-HPG is shown in orange. (d) Docking of the D-HPG into the active site of CgDAPDHBC621/D120S/W144S/I169P. D-HPG is shown in orange, NADP+ cofactor is

shown in cyan, residue S120 is shown in purple, L150 is shown in magenta, G151 is shown in yellow, and H152 is shown in green. The hydrogen-bond between D-HPG and residues S120, L150, G151 and N270 are shown in green dash lines, respectively. The yellow dash lines denote d(C6HDAP–C4NNADP) and d(C6DAP–ND1His152), respectively. (e) Superposition of the D-HPG conformation in parent CgDAPDHBC621 and variant CgDAPDHBC621/D120S/W144S/I169P. (f-g) RMSD values calculated from MD simulations of CgDAPDHBC621 and CgDAPDHBC621/D120S/W144S/I169P. The highlight represented the changes of the region with noticeable movements for CgDAPDHBC621.

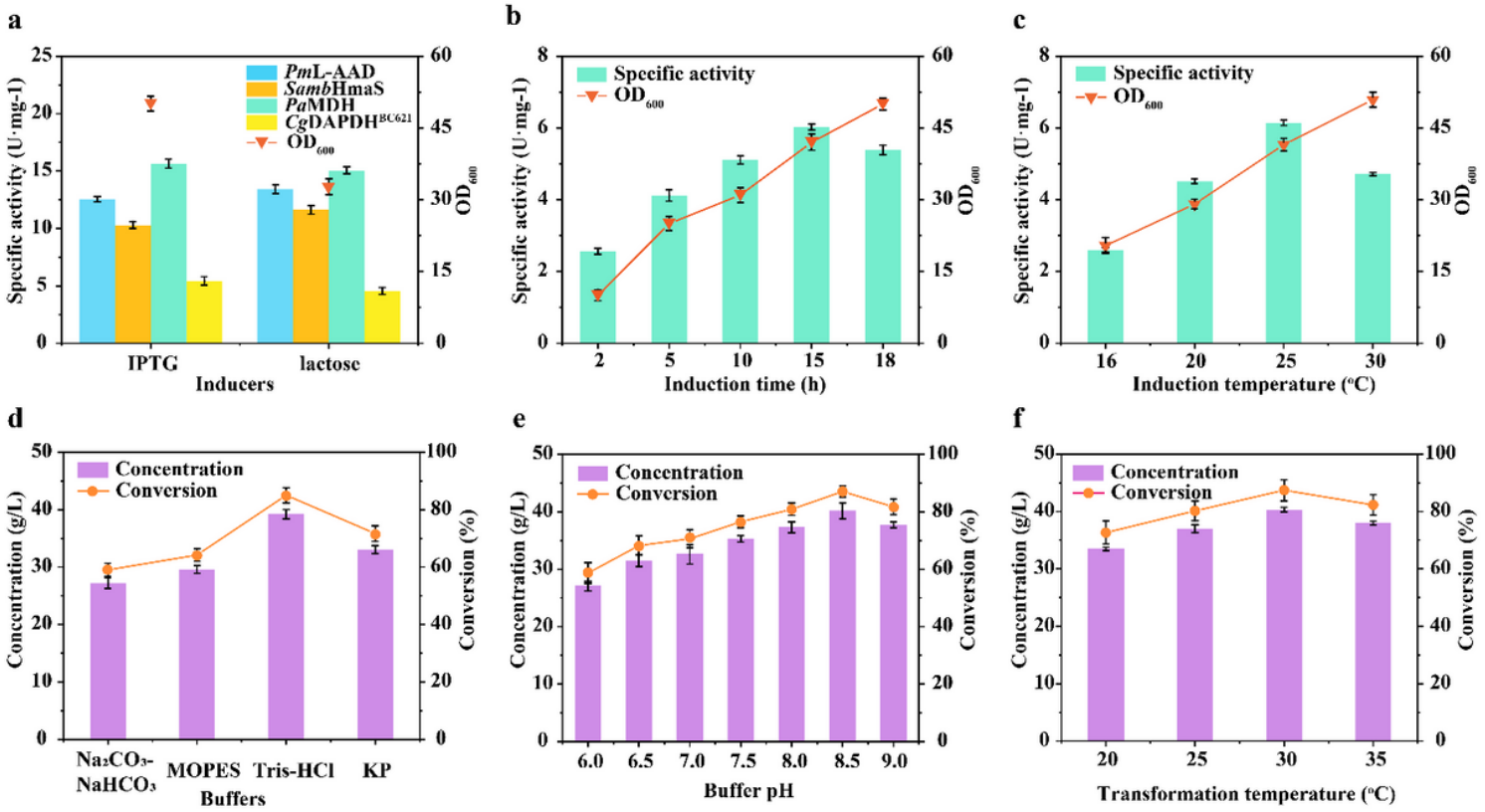

Figure 5

Optimizations during induction and conversion process with strain E. coli 07. (a) Effect of inducers (IPTG and lactose) on specific activity of the four route enzymes and cell growth of E. coli 07. (b) Effect of induction time on CgDAPDHBC621/D120S/W144S/I169P specific activity and cell growth. (c) Effect of induction temperature on CgDAPDHBC621/D120S/W144S/I169P specific activity and cell growth. (d) Effect of buffer type on D-HPG concentration. (e) Effect of buffer pH on D-HPG concentration. (f) Effect of transformation temperature on D-HPG concentration. Reactions were performed in triplicate with resting cells of E. coli 07 (20 g/L wet cells) and 50 g/L L-tyrosine in 800 ml Tris-HCl buffer (20 mM, pH 8.5, 50 g/L NH4Cl, 0.5 mM CoSO4 and 0.7 mM NADP+) at 500 rpm and 30 °C for 24 h. The conversion and titer were obtained after completion of the reactions and determined by HPLC analysis.

Supplementary Files

This is a list of supplementary files associated with this preprint. Click to download.

- Graphicalabstract.docx
- Supportinginformation.docx